IEEE Access
Multidisciplinary | Rapid Review | Open Access Journal

Date of publication xxxx 00, 0000, date of current version xxxx 00, 0000.

Digital Object Identifier 10.1109/ACCESS.2017.DOI

Inter-User Interference Analysis in a Point-to-Multipoint Sub-THz Wireless Communication Link

J. Dittmer[1] (Student Member, IEEE), A. Bhutani[2] (Senior Member, IEEE), C. Bremauer[1] (Student Member, IEEE), F. Beuthan[1], J. Seidel[1], S. Wagner[3], A. Tessmann[3], T. Zwick[2] (Fellow, IEEE), C. Koos[1], S. Randel[1] (Senior Member, IEEE)

[1]Institute of Photonics and Quantum Electronics (IPQ), Karlsruhe Institute of Technology (KIT), Germany.
[2]Institute of Radio Frequency Engineering and Electronics (IHE), Karlsruhe Institute of Technology (KIT), Germany.
[3]Fraunhofer Institute for Applied Solid State Physics IAF, Freiburg, Germany.

Corresponding author: J. Dittmer (e-mail: Joel.Dittmer@kit.edu).

This work was financially supported by the Federal Ministry of Education and Research of Germany in the project "Open6GHub" (grant number: 16KISK010).

ABSTRACT This paper presents the analysis of the inter-user interference (IUI) in a multiuser wireless link operating in the sub-THz frequency range of 270 GHz to 330 GHz. The link utilizes an optoelectronic transmitter (Tx) comprising two integrated external cavity lasers with a wide tuning range, a broadband electro-optic modulator, and a uni-traveling carrier photodiode with a WR3.4 output. A conformal lens-integrated WR3.4 frequency beam-steering antenna transmits the signal to seven users distributed in space. At the user side, an electronic sub-THz receiver is used for the wireless link. A finite portion of the Rx bandwidth (270 GHz to 330 GHz) is allocated to each user. The power ratio between the individual user channels is experimentally evaluated in three different test scenarios, operating at carrier frequencies of 290 GHz, 300 GHz, and 310 GHz, respectively. This evaluation is based on the frequency response analysis of the optoelectronic Tx, the electronic Rx, and the radiation characteristics of the frequency beam-steering antenna. To the best of our knowledge, this work presents the first IUI analysis in a sub-THz wireless link operating over a distance of 10 m, with a record high gross aggregated data rate of 140 Gbps across seven users. A worst-case power ratio of -2.5 dB between adjacent channels and an average power ratio of -11.3 dB is observed, highlighting the potential of sub-THz communication for high-data-rate multiuser networks.

INDEX TERMS 6G, Beam-steering, Interference, Multiuser, Sub-THz, Wireless communication

I. INTRODUCTION

In the era of 6G mobile networks, ultra-high data-rate wireless communication plays a crucial role in enabling applications such as indoor connectivity and outdoor small-cell networks [1, 2]. To accommodate the rapidly increasing demand for bandwidth, high-speed wireless links in the sub-THz range have emerged as a promising solution for future mobile fronthaul networks. These links not only surpass the data rates of 4G and 5G systems but also offer greater flexibility and improved resilience to adverse weather conditions compared to free-space optical links [3]. To promote sub-THz communication, the IEEE has standardized the 253 GHz to 322 GHz range for wireless communication [2]. In particular, the 200 GHz to 325 GHz band stands out as an excellent choice for high-speed wireless links, offering low atmospheric attenuation of less than 10 dB/km in typical weather conditions. Additionally, a wide variety of sub-THz sources have emerged over the past two decades, significantly enhancing the feasibility of deploying the sub-THz range for future wireless applications [4, 5].

The sub-THz range is being targeted for 6G use cases, which operate over short- and medium-range scenarios, typically spanning from a few centimeters to several meters. This is primarily due to the high free-space path loss, which increases quadratically with both frequency and distance. As a result, enhancing the link budget of sub-THz links—by using a transmitter (Tx) with higher output power and a receiver (Rx) with greater sensitivity—becomes crucial. Furthermore, 6G mobile communication systems are expected to achieve significantly higher connection densities compared to 4G and 5G systems. Specifically, 6G aims to support 10 million devices per km^2, in contrast to 2,000 devices per km^2 for 4G and 1 million devices per km^2 for 5G systems [6]. Given the short range and higher device density, close proximity

between neighboring devices is expected in typical 6G use cases. Consequently, the inter-user interference (IUI) among users in close proximity becomes a primary concern. The multiuser sub-THz links demonstrated to date include links based on phased arrays [7, 8] and frequency beam-steering antennas [9–14]. However, none of these published works investigates the channel power ratio between multiple users. The sole exceptions are the crosstalk investigations of a sub-THz link reported in [15] and multiuser link demonstration in [16]. The former focuses on the impact of the frequency-dependent radiation characteristics of a leaky-wave antenna (LWA), while the latter presents experimental and analytical validation of user scaling in a multiuser link employing a single detector and a LWA operating between $180\,\mathrm{GHz}$ and $900\,\mathrm{GHz}$, both conducted in a limited laboratory setup spanning $0.254\,\mathrm{m}$.

Building on the four-user wireless link in [14], this work investigates the IUI, in this case the power ratio between each of the multiple users and extends the number of users to seven. The link consists of an optoelectronic Tx that includes two integrated external cavity lasers with a wide tuning range, a broadband electro-optic modulator, and a uni-traveling carrier photodiode (UTC-PD) with a WR3.4 output. The Tx signal is radiated by a conformal lens-integrated WR3.4 frequency beam-steering antenna, which allows the Tx beam to steer spatially as the operating frequency is tuned within the target sub-THz range. In the presented link data is simultaneously send to seven users distributed in space. An electronic sub-THz Rx is used for the link. A finite portion of the Rx bandwidth ($270\,\mathrm{GHz}$ to $330\,\mathrm{GHz}$) is allocated to each user, thus complementing the concept of a tunable optoelectronic Tx combined with a frequency beam-steering antenna. Power ratios between the users are experimentally evaluated in three different test scenarios, operating at center frequencies of $290\,\mathrm{GHz}$, $300\,\mathrm{GHz}$, and $310\,\mathrm{GHz}$, respectively. This evaluation is based on the frequency response analysis of the optoelectronic Tx, the electronic Rx, and the radiation characteristics of the frequency beam-steering antenna. To the best of the authors' knowledge, this work presents the first adjacent user power ratio analysis of a sub-THz wireless link operating over a distance more than ten times greater than in previous works, achieving the highest gross aggregate data rate of $140\,\mathrm{Gbit/s}$ across seven users in the frequency range of 270-330 GHz [9, 15–21]. The IUI results shown here highlight the potential of sub-THz communication for high-data-rate dense multiuser networks, which could be employed in future 6G use cases.

II. MULTIUSER SUB-THZ WIRELESS LINK

The multiuser sub-THz wireless link operates within the frequency range of $270\,\mathrm{GHz}$ to $330\,\mathrm{GHz}$. Building upon the four-user system presented in [14], this paper investigates the IUI and extends the number of simultaneous users to seven, increasing the aggregated gross data rate to $140\,\mathrm{Gbps}$. A highly tunable optoelectronic Tx, incorporating a WR3.4 frequency beam-steering antenna [22], is employed to generate and radiate the broadband sub-THz signal. The seven sub-THz beams, transmitted to seven spatially separated users are centered at different carrier frequencies and feature finite sub-carrier spacing. Each user receives the sub-THz signal via a broadband, electronic sub-THz Rx, with a finite portion of the Rx bandwidth allocated to each user. The sub-THz Rx thus complements the concept of a tunable optoelectronic Tx with a frequency beam-steering antenna. A schematic of the Tx and Rx is shown in Fig. 2. The Tx and receiver Rx are positioned $10\,\mathrm{m}$ apart. A brief overview of the transmission system is provided below.

A. OPTOELECTRONIC TX AND CONFORMAL LENS INTEGRATED WR3.4 FREQUENCY BEAM-STEERING ANTENNA

The signal is generated in the optical domain using two hybrid-integrated external cavity lasers (ECLs) with a wide tuning range from $1480\,\mathrm{nm}$ to $1570\,\mathrm{nm}$ (i.e., $190.95\,\mathrm{THz}$ to $202.56\,\mathrm{THz}$), an on-chip output power of $12\,\mathrm{dBm}$, and an intrinsic linewidth of less than $1\,\mathrm{kHz}$ [23]. The ECLs generate a carrier signal (ECL1) and a reference signal (ECL2) as required for the optical heterodyning process [24]. In-phase (I) and quadrature (Q) baseband signals with a sampling rate of $120\,\mathrm{GSa/s}$ are modulated onto ECL1 via an electro-optical IQ modulator with an optical $3\,\text{-dB}$ bandwidth of $60\,\mathrm{GHz}$. The modulated optical signal is subsequently amplified by an Erbium-doped fiber amplifier (EDFA), followed by an optical bandpass filter that reduces out-of-band amplified spontaneous emission (ASE) noise generated by the EDFA. The two optical signals are combined in a 50/50

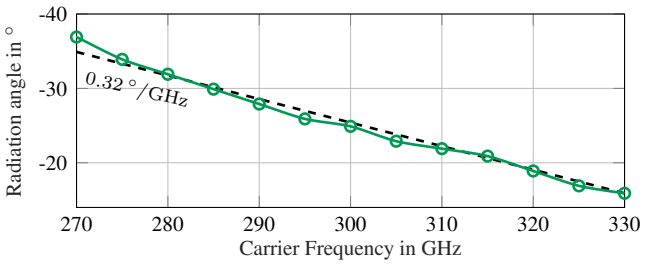

FIGURE 1: Measured radiation angle across the sub-THz range for a conformal lens-integrated WR3.4 frequency beam-steering antenna [22].

coupler, and the total optical power is adjusted by a variable optical attenuator (VOA) before being fed into a broadband photomixing UTC-PD, which requires an input power of $11\,\mathrm{dBm}$ [25]. The resulting sub-THz signal, with a carrier frequency of $270\,\mathrm{GHz}$ to $330\,\mathrm{GHz}$, is radiated by a conformal lens-integrated WR3.4 frequency beam-steering antenna. The WR3.4 frequency beam-steering antenna used in this work operates from $230\,\mathrm{GHz}$ to $330\,\mathrm{GHz}$ and features a wide beam-steering range of $55°$. The antenna is integrated with a polytetrafluoroethylene (PTFE)-based conformal plano-convex parabolic lens, which achieves a peak antenna gain of up to $30\,\mathrm{dBi}$ [22]. The WR3.4 antenna operates based on the leaky-wave principle, allowing its beam to steer from $-71°$ to $-16°$ relative to broadside direction as the operating

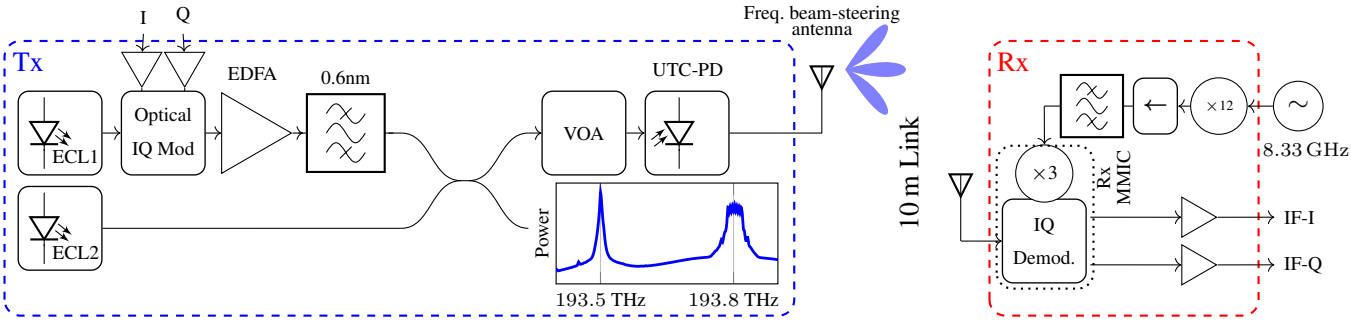

FIGURE 2: Schematic of a multiuser sub-THz wireless link, featuring a highly tunable optoelectronic Tx connected to a frequency beam-steering antenna (left) and a broadband electronic Rx (right). Note: The frequencies shown in the figure correspond to a center frequency of 300 GHz. (Adapted from [14])

frequency sweeps from 230 GHz to 330 GHz. A detailed description of the antenna, including its design principle, simulation, and measurement, is provided in [22]. Since the multiuser sub-THz link operates from 270 GHz to 330 GHz, the corresponding radiation angle of the WR3.4 frequency beam-steering antenna varies from $-31°$ to $-19°$, respectively (see Fig. 1). The frequency tunable optoelectronic Tx and the conformal lens integrated WR3.4 frequency beam-steering antenna are shown in Fig. 2 and Fig. 3, respectively.

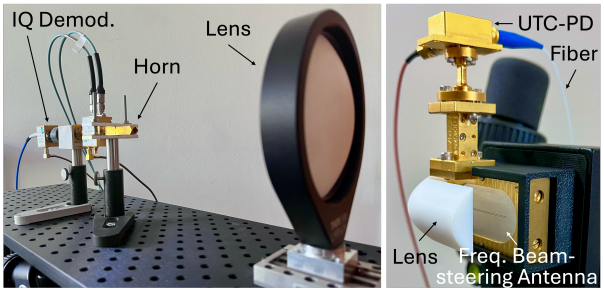

FIGURE 3: Optoelectronic Tx and conformal-lens-integrated WR3.4 frequency beam-steering antenna (right). Electronic Rx and lens-integrated WR3.4 horn antenna (left).

B. ELECTRONIC RX AND LENS INTEGRATED WR3.4 HORN

At the core of the used electronic Rx is a 300 GHz monolithic microwave integrated circuit (MMIC), which consists of a low-noise preamplifier, a frequency tripler, and a subharmonic IQ demodulator. The sub-THz signal is received by a WR3.4 horn integrated with a PTFE-based spherical plano-convex lens. This signal is then down-converted by the IQ demodulator into intermediate frequency in-phase (IF-I) and quadrature (IF-Q) signals. The Rx MMIC requires a 100 GHz local oscillator (LO) signal for the demodulation. This LO signal is generated from an 8.333 GHz signal produced by a frequency synthesizer, which is upconverted by a $\times 12$ frequency multiplier [26]. The LO signal passes through a waveguide isolator to prevent reflections into the frequency multiplier, which could cause unwanted frequency drifts and harmonics. These harmonics are further suppressed using a waveguide bandpass filter. The measured conversion gain of the Rx module spans from -5 dB to 5 dB across an IF bandwidth of 40 GHz. A detailed description of the sub-THz Rx module is provided in [27]. The IF-I and IF-Q signals are preamplified by two broadband RF amplifiers and sampled by two channels of a 32 GHz bandwidth real-time oscilloscope.

III. EXPERIMENTAL SETUP FOR LEAKAGE ANALYSIS

In our experimental setup, the IUI is defined as IUI $= P_{\mathrm{AU}}/P_{\mathrm{TU}}$ between the adjacent user (AU) and the target channel (TU) and is analyzed for a total of seven users/channels. These users are separated in both the spatial and spectral domains due to the frequency beam-steering concept employed on the Tx side (as described in Section II). The Tx antenna has a half-power beam width (HPBW) of approximately 9.5 GHz [22], which limits the maximum signal bandwidth that can be transmitted to each user. As a result, the antenna beam characteristics mainly influence the power received by each neighboring user.

On the Rx side, each user is assigned a finite portion of the Rx bandwidth (270 GHz to 330 GHz), meaning each user is allocated a specific center frequency and a finite signal bandwidth. Furthermore, a guard band is used to separate neighboring users, preventing spectral overlap between adjacent users. To analyze the IUI between seven users in a frequency beam-steering-enabled sub-THz wireless link, the following key factors are evaluated:

- The power received by the adjacent users distributed in the spatial and spectral domains.
- The radiation characteristics of the frequency beam-steering antenna employed on the Tx side, including its beam gain and beam width.
- The frequency responses of the optoelectronic Tx and the electronic Rx.

To experimentally evaluate these factors, three different test scenarios were set up. The Tx spectra for these scenarios, labeled Scenario 1, Scenario 2, and Scenario 3, are shown in Fig. 4. The target user (TU) is located at a center frequency of 290 GHz (Sce. 1), 300 GHz (Sce. 2), and 310 GHz (Sce. 3). In each scenario, there are six non-intended adjacent users (AU): three are positioned in the lower sub-THz range and the remaining three are located in the upper sub-THz range rela-

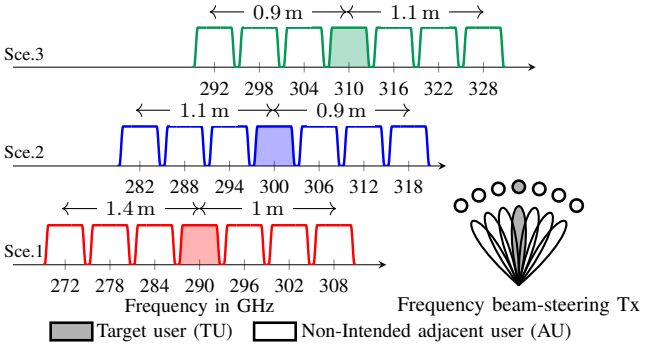

FIGURE 4: Tx spectra for three test scenarios (Sce. 1 , Sce. 2, and Sce. 3), each involving seven users (left) and spectral distribution of the users (right).

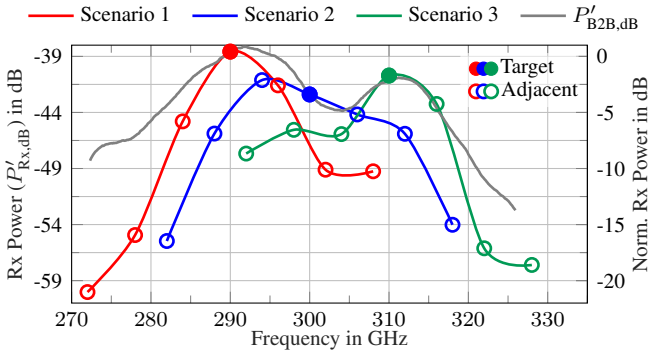

FIGURE 5: Rx power and normalized Rx Power for the target and six adjacent user channels for the three angular/frequency scenarios.

tive to the center frequency of the TU. The signal transmitted to each user is modulated using quadrature phase-shift keying (QPSK) and 16-level quadrature amplitude modulation (16-QAM), with a symbol rate of 5 GBd in both cases. The signal is shaped using a root-raised cosine filter with a roll-off factor of 0.1, resulting in an effective signal bandwidth of 5.5 GHz per user. Additionally, a 0.5 GHz guard band is employed between neighboring users, which results in a subcarrier spacing of 6 GHz (5.5 GHz + 0.5 GHz) between adjacent users. The Tx spectra of the seven users in the three scenarios are shown in Fig. 4. Due to the frequency beam-steering capability of the Tx, the spectral distribution of the seven users results in an angular separation between them. As analyzed using Fig. 1 and Fig. 4, the users are positioned at angles ranging from $-37°$ to $-22°$ in Sce. 1, $-32°$ to $-19°$ in Sce. 2, and $-28°$ to $-16°$ in Sce. 3. For a link distance of 10 m, the angular separation between the target and the AUs leads to a lateral separation, as shown in Fig. 4 for the three scenarios. The sub-THz Rx is aligned to receive the maximum power corresponding to the TU in each test scenario. Due to the broad operating bandwidth of the Rx, the received power is evaluated for subcarriers associated with all seven users (see Fig. 4). This setup allows for the evaluation of the power ratio between the target and the AUs, and consequently, the leakage between the users. Additionally, the signal performance is evaluated based on the received signal's signal-to-noise-and-distortion ratio (SNDR) and bit error ratio (BER) after offline, non-data-aided digital signal processing. The measured power and SNDR are also analyzed in relation to the radiation characteristics of the conformal lens-integrated WR3.4 frequency beam-steering antenna.

IV. LEAKAGE MEASUREMENT RESULT AND ANALYSIS

For the three scenarios, i.e., Sce. 1, 2, and 3, the IUI from the AUs to the TU is evaluated by extracting the spectral power of each subcarrier after signal detection in the sub-THz receiver. The resulting power ($P_{\mathrm{Rx,dB}}$) and normalized power received by the sub-THz Rx, corresponding to the TU and the six AUs is given in Fig. 5. The power ratio between the TU and the AUs can be analyzed from this figure. For example, in Sce. 1, the IUI between the TU at 290 GHz and the AU at 308 GHz is -11 dB, indicated by the normalized receive power at 308 GHz by the receiver assigned a center frequency of 290 GHz. These two users have a lateral separation of 1 m (see Fig. 4). To evaluate the influence of the frequency responses of the optoelectronic Tx and electronic Rx, a back-to-back (B2B) measurement is conducted. The output (OP) WR3.4 flange (WF) of the UTC-PD connects to the input (IP) WF of the attenuator, whose OP-WF connects to the IP-WF of the Rx. All WFs conform to the UG-387/U-M standard, ensuring seamless interfacing. The attenuator is adjusted to replicate the influence of the Tx and Rx antenna gain and the free-space path loss corresponding to a link distance of 10 m. The Tx-Rx B2B frequency response ($P_{\mathrm{B2B,dB}}$) is shown in gray in Fig. 5. As shown in the figure, $P_{\mathrm{Rx,dB}}$ of the TUs at 290 GHz, 300 GHz, and 310 GHz (solid dots) closely matches the corresponding $P_{\mathrm{B2B,dB}}$. This suggests that the power level received by the TUs is primarily influenced by the frequency response of the Tx and Rx. In contrast, the values of $P_{\mathrm{Rx,dB}}$ observed at the locations of the six AUs, situated on either side of the TU in each scenario, show a deviation relative to $P_{\mathrm{B2B,dB}}$. For example, in Sce. 1, the values of $P_{\mathrm{Rx,dB}}$ at 272 GHz, 278 GHz, 284 GHz, 296 GHz, 302 GHz, and 308 GHz (corresponding to the six AUs) exhibit a deviation of up to 12 dB w.r.t $P_{\mathrm{B2B,dB}}$. This deviation can be explained as follows: As described in Section III, the Rx is aligned to capture the maximum power corresponding to the TU in each scenario. In these scenarios, the TU receives power from the main lobe of the antenna's far-field radiation pattern at the center frequency of the TU, while the six AUs receive power from the side lobes of the far-field radiation pattern at the same frequency. Therefore, the power of the AUs received by a TU is influenced not only by the frequency responses of the Tx and Rx but also by the radiation characteristics of the frequency beam-steering antenna. To analyze the influence of the frequency beam-steering antenna, the antenna's far-field radiation pattern is measured at 290 GHz, 300 GHz, and 310 GHz for Sce. 1, 2, and 3, respectively. Additionally, the calibrated IUI is calculated for each of the three scenarios to de-embed the influence of the Tx-Rx B2B frequency response on the overall IUI: Calibrated $\mathrm{IUI_{dB}} = P_{\mathrm{Rx,dB}}(f) - P_{\mathrm{B2B,dB}}(f)$. The measured far-field radiation patterns of the conformal lens-integrated

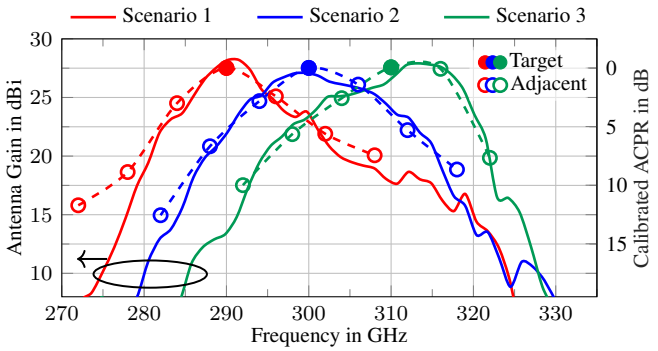

FIGURE 6: Antenna gain (solid line, left axis) and calibrated IUI (dashed line, right axis) for the target and six adjacent users for the three scenarios.

frequency beam-steering antenna and the calibrated IUI calculated for the three scenarios are shown in Fig. 6. In contrast to Fig. 5, the de-embedded IUI corresponding to the TUs in the three scenarios remains relatively constant, as the measured gain of the antenna's main lobe varies slightly from 27.1 dB to 27.9 dB. On the other hand, in Fig. 5, the $P_{\mathrm{Rx,dB}}$ of the TUs varies by up to 4.8 dB. This implies that the power received by the TUs is largely influenced by the Tx-Rx B2B frequency response, provided the antenna gain remains practically constant over the target sub-THz range. Furthermore, in Fig. 6, the calibrated IUI corresponding to the six AUs closely matches the antenna's far-field radiation patterns at 290 GHz, 300 GHz, and 310 GHz for Sce. 1, 2, and 3, respectively. This indicates that the power from the six AUs received by the TU is significantly influenced by the radiation characteristics of the frequency beam-steering antenna. The worst-case leakage is -2.5 dB, observed between a TU and its AU with a lateral separation of around 0.4 m. For larger lateral separations, a best-case leakage of -22 dB is observed. An exception is observed in Fig. 5, where the TU at 300 GHz receives slightly less $P_{\mathrm{Rx,dB}}$ than the AU at 294 GHz, attributed to the reduced frequency response of the Rx at around 300 GHz (see Fig. 5). Neglecting the Tx–Rx response, the IUI, expressed in dB, exhibits a dependence on the channel offset Δf and is the antenna's HPBW, both expressed in GHz, as

$$\mathrm{IUI_{dB}} \approx -\frac{3\,\mathrm{dB/GHz}}{\mathrm{HPBW_{GHz}}}\Delta f^2_{\mathrm{GHz}} - 1\,\mathrm{dB}\,. \tag{1}$$

This indicates that with increased subcarrier spacing Δf or reduced HPBW the IUI is decreased. The performance of a 10 m-long wireless communication link using 5 GBd QPSK and 16-QAM modulation schemes is evaluated. The measured SNDR and BER for the scenarios are shown in Fig. 7. In each scenario, the peak SNDR is observed for the TU, which varies from 14.7 dB for the TU at 290 GHz (Sce. 1) to 13.2 dB for the TUs at 300 GHz and 310 GHz (Sce. 2 and 3) for QPSK. For 16-QAM, a slight SNDR degradation of up to 0.3 dB is observed, attributed to its higher susceptibility to nonlinear effects. As a result, for 16-QAM, only the signal from AUs with a small lateral separation of 0.4 m can be decoded after non-data-aided DSP in the TU, leading to a BER above the soft-decision forward error correction (SD-FEC) threshold of 2.4×10^{-2}. However, a BER below this threshold can be corrected with a 20% coding overhead, for example, using low-density parity-check (LDPC) codes [28, 29]. On the other hand, signals from AUs with larger lateral separations cannot be decoded since the IUI is significantly higher. In contrast, QPSK has a higher tolerance to noise and nonlinearities, which enables the decoding of signals of AUs at lateral separations of up to 0.4 m with a BER below the SD-FEC limit in Sce. 1, 2, and 3. To the best of the authors' knowledge, the shown experiment presents a record-high aggregated gross data rate of 7 Users $\times$ 5 GBd $\times$ 4 bit/sym $=$ 140 Gbit/s for 16-QAM and 70 Gbit/s for QPSK.

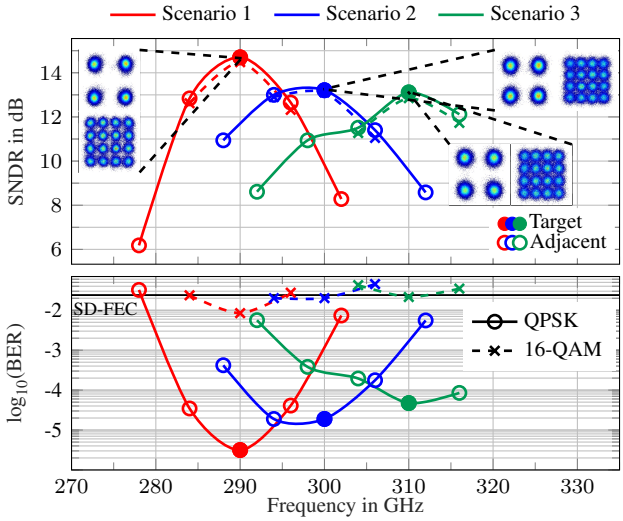

FIGURE 7: SNDR and BER in three test scenarios using 5 GBd QPSK and 16-QAM modulation.

V. CONCLUSION

This paper presents an inter-user interference (IUI) analysis in a sub-THz wireless link with one target user (TU) and six non-intended adjacent users (AU) across three different test scenarios at center frequencies of 290 GHz, 300 GHz, and 310 GHz. The 10 m-long multiuser link operates from 270 GHz to 330 GHz and consists of an optoelectronic Tx with a conformal lens-integrated WR3.4 frequency beam-steering antenna, and an electronic Rx combined with a lens-integrated WR3.4 horn antenna. For the power ratio analysis, the Rx power of the seven users is compared with the frequency response of the Tx and Rx, as well as the far-field radiation pattern of the frequency beam-steering antenna. The results show that the power received by the TU is primarily influenced by the frequency response of the Tx and Rx, assuming the antenna gain remains nearly constant across the target sub-THz range. Additionally, the signal power from the six AUs received by the TU is mainly influenced by the far-field radiation characteristics of the frequency beam-steering antenna. In each of the three scenarios, the IUI ranges from -2.5 dB to -22 dB, depending on the spectral and consequently lateral separation of the users. The performance evaluation of the 10 m-long communication

link using $5\,\mathrm{GBd}$ QPSK and 16-QAM demonstrates that the SNDR of the TU varies between $14.7\,\mathrm{dB}$ and $13.2\,\mathrm{dB}$. This results in a BER below the SD-FEC limit of 2.4×10^{-2} for all TUs and AUs with a maximum separation of $0.4\,\mathrm{m}$ when using QPSK, and for the TU only when using 16-QAM. To the best of the authors' knowledge, this work presents the first insight IUI analysis in a sub-THz link spanning several meters, where simultaneous transmission to seven users is achieved with a maximum aggregated gross data rate of $140\,\mathrm{Gbit/s}$. The IUI analysis quantifies the tradeoff between data rate and user density imposed by adjacent user power requirements and guard-band constraints in dense sub-THz multiuser systems. It reveals the inherent coupling between transmit power, bandwidth, user capacity, and modulation format in high-capacity sub-THz multiuser links.

AUTHOR CONTRIBUTION

The conceptualization of this work was done by J. Dittmer and A. Bhutani. The system-level experiments were conducted by J. Dittmer, C. Bemauer, F. Beuthan, and J. Seidel. The paper was written and revised by J. Dittmer and A. Bhutani. C. Bremauer manufactured the laser diodes. J. Dittmer and A. Bhutani assembled the transmit antenna. S. Wagner and A. Tessmann provided the Rx module. The funding for this work was acquired by A. Bhutani, C. Koos, T. Zwick, and S. Randel.

References

[1] CISCO, "Cisco Annual Internet Report (2018–23)," *White Pap.*, 2020.

[2] V. Petrov et al., "IEEE 802.15.3d: First Standardization Efforts for Sub-Terahertz Band Communications toward 6G," *IEEE Communications Magazine*, vol. 58, no. 11, pp. 28–33, 2020.

[3] M. Shehata et al., "Optical and Terahertz Wireless Technologies: the Race to 6G Communications," *IEEE Wirel. Commun.*, vol. 30, no. 5, pp. 10–18, 2023.

[4] K. Sano et al., "Ultra-fast optoelectronic circuit using resonant tunnelling diodes and unitravelling-carrier photodiode," *Electronics Letters*, vol. 34, no. 2, pp. 215–217, 1998.

[5] H. Hamada et al., "Millimeter-wave InP Device Technologies for Ultra-high Speed Wireless Communications toward Beyond 5G," *2019 IEEE Int. Electron Devices Meet. (IEDM)*, pp. 9.2.1–9.2.4, 2019.

[6] M. Banafaa et al., "6G Mobile Communication Technology: Requirements, Targets, Applications, Challenges, Advantages, and Opportunities," *Alexandria Engineering Journal*, vol. 64, pp. 245–274, 2023.

[7] Y. Yang et al., "An eight-element 370–410-GHz phased-array transmitter in 45-nm CMOS SOI with peak EIRP of 8–8.5 dBm," *IEEE Trans. Micro. Theory Techn.*, vol. 64, no. 12, pp. 4241–4249, 2016.

[8] P. Lu et al., "Photonic assisted beam steering for millimeter-wave and THz antennas," *2018 IEEE Conf. Antenna Meas. Appl. (CAMA)*, pp. 1–4, 2018.

[9] P. Lu et al., "Mobile THz communications using photonic assisted beam steering leaky-wave antennas," *Opt. Express*, vol. 29, no. 14, pp. 21 629–21 638, 2021.

[10] K. Sarabandi et al., "A novel frequency beam-steering antenna array for submillimeter-wave applications," *IEEE Trans. Terahertz Sci. Technol.*, vol. 8, no. 6, pp. 654–665, 2018.

[11] K. Murano et al., "Low-profile terahertz radar based on broadband leaky-wave beam steering," *IEEE Trans. Terahertz Sci. Technol.*, vol. 7, no. 1, pp. 60–69, 2016.

[12] J. Tebart et al., "Point-to-multipoint beam-steering terahertz communications using a photonics-based leaky-wave transmit antenna," *Int. J. Micro. Wireless. Technol.*, pp. 1–9, 2024.

[13] T. Haddad et al., "THz Optoelectronic 2-D Beam Steering Transmitter for Short-Range Communications," *2024 15th German Microwave Conference (GeMiC)*, pp. 300–303, 2024.

[14] J. Dittmer et al., "Multi-User Long-Distance sub-THz Wireless Communication," *IEEE Trans. Terahertz Sci. Technol.*, pp. 1–11, 2025.

[15] C.-Y. Yeh et al., "Security and Angle-Frequency Coupling in Terahertz WLANs," *IEEE/ACM Transactions on Networking*, vol. 32, no. 2, pp. 1524–1539, 2024.

[16] K. P. Dasala and E. W. Knightly, "Multi-user terahertz WLANs with angularly dispersive links," *Proc. 23rd Int. Symp. Theory, Algorithmic Found., Protocol Des. Mobile Netw. Mobile Comput.*, MobiHoc '22, pp. 121–130, 2022.

[17] I. Abdo et al., "A bi-directional 300-GHz-band phased-array transceiver in 65-nm CMOS with out-phasing transmitting mode and LO emission cancellation," *IEEE Journal of Solid-State Circuits*, vol. 57, no. 8, pp. 2292–2308, 2022.

[18] B. Yu et al., "A 200-GHz four-element phased-array receiver system-in-package using HTCC technology for sub-terahertz communications," *IEEE Transactions on Microwave Theory and Techniques*, vol. 72, no. 7, pp. 3920–3934, 2023.

[19] J. Tebart et al., "Mobile 6G communications at THz frequencies enabled by leaky-wave antenna beam steering," *2023 53rd European Microwave Conference (EuMC)*, pp. 142–145, 2023.

[20] J. Hebeler et al., "Wideband BPSK Transmitter Phased Array Operating at 246 GHz With±30° Steering Range," *IEEE Access*, 2024.

[21] O. Stiewe et al., "Towards High-Capacity THz-Wireless P2MP Communication Systems for 6G," in *2022 52nd European Microwave Conference (EuMC)*, IEEE, 2022, pp. 40–43.

[22] A. Bhutani et al., "Sub-THz Conformal Lens Integrated WR3.4 Antenna for High-Gain Beam-Steering," *IEEE IEEE Open J. Antennas Propag.*, vol. 5, no. 5, pp. 1306–1319, 2024.

[23] P. Maier et al., "Sub-kHz-Linewidth External-Cavity Laser (ECL) With Si3N4 Resonator Used as a Tunable

Pump for a Kerr Frequency Comb," *J. Light. Technol.*, vol. 41, no. 11, pp. 3479–3490, 2023.

[24] J. Dittmer et al., "Comparison of electronic and optoelectronic signal generation for (sub-) THz communications," *Int. J. Micro. Wireless. Technol.*, pp. 1–11, 2024.

[25] H. Ito et al., "Uni-traveling-carrier photodiodes for high-speed detection and broadband sensing," *Quantum Sensing and Nanophotonic Devices IV*, vol. 6479, p. 64790X, 2007.

[26] I. Kallfass et al., "MMIC chipset for 300 GHz indoor wireless communication," *2015 IEEE Int. Conf. Microw., Commun., Antennas Electron. Syst. (COMCAS)*, pp. 1–4, 2015.

[27] I. Kallfass et al., "Towards MMIC-based 300GHz indoor wireless communication systems," *IEICE transactions on electronics*, vol. 98, no. 12, pp. 1081–1090, 2015.

[28] A. Leven and L. Schmalen, "Status and recent advances on forward error correction technologies for lightwave systems," *J. Light. Technol.*, vol. 32, no. 16, pp. 2735–2750, 2014.

[29] D. A. Morero et al., "Non-concatenated FEC codes for ultra-high speed optical transport networks," in *2011 IEEE Global Telecommunications Conference-GLOBECOM 2011*, IEEE, 2011, pp. 1–5.

JOEL DITTMER was born in Karlsruhe, Germany, in 1995. He received the B.Sc. and M.Sc. degrees in electrical engineering from the Karlsruhe Institute of Technology, Karlsruhe, Germany, in 2020 and 2022, respectively. He joined the Institute of Photonics and Quantum Electronics (IPQ) at the Karlsruhe Institute of Technology in 2023, where he started as a research assistant in the field of optoelectronic and electronic generated Terahertz signals for wireless communications. His research interests include THz system design, THz package design, and high data rate digital signal processing.

AKANKSHA BHUTANI earned her M.Sc. and Ph.D. in Electrical Engineering and Information Technology from the Karlsruhe Institute of Technology (KIT), Germany, in 2012 and 2019, respectively. Since 2019, she has been leading the Antennas and Packaging research group at KIT's Institute of Radio Frequency Engineering and Electronics. Her work focuses on THz antennas and packaging for radar and wireless communication. Bhutani's accolades include the "Carl Freudenberg Prize" and the "Südwestmetall Advancement Award" for her dissertation in 2019 and 2020, the IEEE Microwave Magazine Best Paper Award in 2017, and the European Microwave Week (EuMW) Best Paper Awards in 2019 and 2022 and the International IHP "Wolfgang Mehr" Fellowship Award by the Leibniz-Institut für innovative Mikroelektronik (IHP) in 2023. In 2023, she served as the Operations Officer of EuMW 2023 held in Berlin. She has authored and co-authored over 50 research papers.

CHRISTIAN BREMAUER received his M.Sc. in electrical engineering from the Karlsruhe Institute of Technology (KIT), Karlsruhe, Germany, in 2017. From 2018 to 2020, he worked as a test engineer at Keysight Technologies in Böblingen, Germany. In 2020, he joined the Institute of Photonics and Quantum Electronics (IPQ) at the KIT, where he is currently working as a research associate. His research interests include optical metrology, photonic integration, and packaging.

FELIX BEUTHAN is currently pursuing his master's degree in electrical engineering at the Institute of Photonics and Quantum Electronics at the Karlsruhe Institute of Technology. He is currently working as a research assistant with his focus on terahertz communication technologies. His research interests and experiences include optical communication systems, terahertz technologies and their applications in advanced communication networks.

JOSEFINE SEIDEL is currently pursuing her bachelor's degree in electrical engineering at the Institute of Photonics and Quantum Electronics at the Karlsruhe Institute of Technology. She is currently working on her bachelor's thesis on mobile users for terahertz communication. Her research interests and experience include terahertz technologies and satellite communication.

SANDRINE WAGNER received a B.Sc. in Electronics and Informatics from the University of Mulhouse, France in 1989. She joined Micronas GmbH in Freiburg, Germany in 1989 where she was responsible for layout and physical verification of large scale integrated semi-conductor devices. In 2010 she joined the Fraunhofer Institute for Applied Solid State Physics (IAF), Freiburg, Germany. Her main interest is the measurement of high frequency nonlinear circuits.

AXEL TESSMANN received the Dipl.-Ing. degree in electrical engineering from the University of Karlsruhe, Germany, in 1997 and the Ph.D. degree in electrical engineering from the University of Karlsruhe, Germany, in 2006. In 1997, he joined the Microelectronics Department, Fraunhofer Institute for Applied Solid State Physics (IAF), Freiburg, Germany, where he is involved in the development of monolithically integrated circuits and subsystems for high-resolution imaging systems and high data rate wireless communication links. His main research areas are the design and packaging of millimeter-wave and submillimeter wave ICs as well as circuit simulation and linear and nonlinear device modeling. He is currently Group Manager of the millimeter wave packaging and subsystem group at the Fraunhofer IAF.

THOMAS ZWICK (Fellow, IEEE) received the Dipl.-Ing. (M.S.E.E.) and the Dr.-Ing. (Ph.D.E.E.) degrees from the University Karlsruhe (TH), Germany, in 1994 and 1999, respectively. From 1994 to 2001 he was a research assistant at the Institut für Hochstfrequenztechnik und Elektronik (IHE) at the University Karlsruhe (TH), Germany. In February 2001 he joined IBM as research staff member at the IBM T. J. Watson Research Center, Yorktown Heights, NY, USA. From October 2004 to September 2007, Thomas Zwick was with Siemens AG, Lindau, Germany. During this period he managed the RF development team for automotive radars. In October 2007, he became a full professor at the Karlsruhe Institute of Technology (KIT), Germany. He is the director of the Institut für Hochfrequenztechnik und Elektronik (IHE) at the KIT.

CHRISTIAN KOOS received the Ph.D. (Dr.-Ing.) degree in electrical engineering from the University of Karlsruhe, Karlsruhe, Germany, in 2007. He is currently a full Professor with the Karlsruhe Institute of Technology, Karlsruhe, Germany, where he is heading the Institute of Photonics and Quantum Electronics. He has co-founded several start-up companies, such as Vanguard Photonics GmbH, Vanguard Automation GmbH, SilOriX GmbH, and DeepLight SA. From 2008 to 2010, he was affiliated with the Corporate Research and Technology Department of Carl Zeiss AG in Oberkochen, Germany, where he led the technology forecast in the area of nanotechnology. He is the author of more than 140 journal papers and more than 30 patent families. His research interests include silicon photonics and hybrid integration concepts along with the associated applications in high-speed communications, optical sensing and metrology, and ultra-fast photonic-electronic signal processing. He was the recipient of several research awards and prestigious grants, such as the ERC Starting Grant in 2011 and ERC Consolidator Grant in 2017.

SEBASTIAN RANDEL (Senior Member, IEEE) received the Dr.-Ing. degree for his work on high-speed optical-time-division-multiplexed transmission systems from Technische Universität Berlin, Berlin, Germany, in 2005. He is currently a full Professor with the Karlsruhe Institute of Technology, Karlsruhe, Germany, where he is co-heading the Institute of Photonics and Quantum Electronics. From 2005 to 2010, he was a Research Scientist with Siemens Corporate Technology, Munich, Germany, where he led research and standardization activities in the fields of polymer-optical-fiber communications, visible-light communications, and optical access networks. From 2010 to 2016, he was a Member of Technical Staff with Bell Laboratories, Holmdel, NJ, USA. His current research focuses on high-capacity power-efficient optical and sub-THz communication systems and networks.